scientific reports

Check for updates

OPEN

Low molecular weight fucoidan differentiation media enhances quality and extents shelf life of 3D human skin model

Yun-Mi Jeong[1]✉, Won-Soo Yun[1] & Jin-Hyung Shim[1,2]✉

In vitro three-dimensional artificial human skin models (3D-HSMs) have revolutionized research in drug testing, disease modeling, and cosmetic evaluations. However, preserving the shelf-life of 3D-HSM during extended culture remains a challenge. Our previous study uncovered the anti-proliferative effect of fibroblasts exposed to low-molecular-weight fucoidan (LMW-F) at a lower concentration. Based on this study, we developed growth and differentiation media with LMW-F to extend 3D-HSM shelf-life. Two specifically designed media types supplemented with LMW-F components were formulated: (1) growth media (DFR-GM) consisting of DMEM (low glucose), Ham's F-12 K, and RPMI 1640 in a precise 2:2:1 ratio, with (LMW-F-DFR-GM) or without LMW-F (con-DFR-GM), and (2) differentiation media (DFR-DM) consisting of the same composition of DFR-GM with the addition of CaCl2, with (LMW-F-DFR-DM) or without LMW-F (con-DFR-DM). Human cell-based 3D-full-thickness HSE model (3D-FT-HSEM) was incubated with these media for 28 days. In comparison to the control group, the 3D-FT-HSEMs cultured in LMW-F supplemented medium showed a 47% reduction in diameter and retained 25% of their thickness (compared to a 94% reduction and complete degradation in the control group), along with enhanced expression of Ki67 proliferation marker (by approximately 20% at day 21) and reduced cell death. Overall, the present study provides valuable insights into enhancing the quality and extending the shelf-life of 3D-FT-HSEMs.

Keywords Low-molecular-weight fucoidan, An alternative to animal testing, Human cell-based 3D-full-thickness artificial human skin models, Long-term cultivation, Prolonged shelf life

Despite the widespread use of animal models in various biomedical research fields, significant disparities exist between animal skin and human skin[1,2]. Animal skin differs significantly from human skin in terms of thickness, collagen types, blood vessel density, and immune cell distribution. These species-specific differences can substantially affect the percutaneous absorption, metabolic processes, and potential toxicological responses of substances. For instance, certain drugs may exhibit high absorption rates in animal skin but low absorption rates in human skin, frequently leading to failures in clinical trials. To address these issues, the development of in vitro models that more accurately mimic human skin is essential. The 3D-FT-HSEM developed in this study can overcome the limitations of animal models and enable more accurate predictions by replicating the structural and functional characteristics of human skin[1,2]. To comply with European, UK, and US regulations, researchers and the medical industry must explore alternative methodologies before turning to animal testing[2]. In vitro three-dimensional artificial human skin models (3D-HSMs) is one promising approach to modeling biological processes in more physiologically relevant ways with a range of applications including drug development, toxicity screening, and regenerative medicine[3]. In particular, the human cell-based 3D full-thickness skin equivalent model (3D-FT-HSEM) is designed to more accurately replicate the structure and function of human skin. While existing in vitro skin models often include only the epidermal layer or fail to adequately represent the structural complexity of the dermal layer, the 3D-FT-HSEM developed in this study includes both the epidermis and dermis and forms a 3D structure similar to actual skin, enabling more accurate research[4–7]. This model features a polycarbonate membrane and a fibroblast-collagen hydrogel-dermal layer, with epidermal keratinocytes cultured in an air–liquid interface. These cells undergo successful differentiation and keratinization to form distinct epidermal sublayers. 3D-FT-HSEM has also been found to be useful for evaluating the effectiveness of

[1]Department of Mechanical Engineering, Tech University of Korea, 237 Sangidaehak Street, Si- heung City, Republic of Korea. [2]Research Institute, T&R Biofab. Co. Ltd, 242 Pangyo-ro, Seongnam 13487, Gyeonggi, Republic of Korea. ✉email: phdjeongym12@tukorea.ac.kr; happyshim@tukorea.ac.kr

new medical devices and materials[4–7]. For instance, EpiSkin™, advanced Skin Test 2000 (AST2000), and EFT-300 FT are commercially available as realistic models for studying skin processes[4–7].

The choice of culture medium impacts two important factors in the development of 3D-HSMs: the formation and organization of the necessary epidermal and dermal layers. Furthermore, while different cell types have been included in various cell culture systems depending on the application, strategies for inclusion—which may involve scaffolds, cell sources, culture media, and/or culture times—remain highly heterogeneous[8–12]. Challenges persist regarding the quality and extension of the shelf-life of artificial skin substitutes, specifically dermal layer-scaffold stability and the health of each cell type within the 3D-HSM culture system[13]. Primary cells, essential for conventional 3D-HSM fabrication, are expensive and slow-growing, and require costly specialized media for cultivation[13]. This study focused on developing cost-effective media formulations using LMW-F, low-glucose DMEM, Ham's F-12 K, and RPMI 1640 to enhance the longevity and stability of 3D FT-HSEMs generated from commercially available cell lines (HaCaT keratinocytes and CCD-986sk fibroblasts). To assess the efficacy of these formulations, we evaluated the impact of LMW-F-supplemented media on the expression of shelf-life-related genes and proteins.

Results

LMW-F-DFR-DM stably enhances the preservation of 3D-FT-HSEMs under long-term culture conditions

The limitations of current commercially available 3D-FT-HSEM systems for long-term studies (around one week ± 5 days) involve issues such as collagen gel-based matrix contraction over time and cell death, which could be influenced by culture media[14]. To overcome these challenges, we developed a novel cost-effective long-term in vitro 3D-FT-HSEM media composition and methods using LMW-F, DMEM (low glucose), Ham's F-12 K, and RPMI 1640 supplemented with (LMW-F-DFR-DM) or without $CaCl_2$ (LMW-F-DFR-GM)(Fig. S1A). For the preparation of the 3D-FT-HSEMs from the commercially available cell lines (HaCaT cells and CCD-986sk cells), we constructed a 3D dermal layer-on-frame structure through layer-by-layer deposition of dermal bioink (collagen I hydrogel with CCD-986sk cells) using a 3D printer (Fig. S1B–S1D). The living constructed dermal layers were randomly divided into the con-DFR-GM group and the LMW-F-DFR-GM group ($n = 10$ each), and then each group was pre-incubated in their respective media for 2 days (Fig. S1D). Next HaCaT cells were seeded on the living dermal layer-on-frame structure and cultured in replaced con-DFR-GM or LMW-F-DFR-GM for 2 days (Fig. S1E). Subsequently, the living completed 3D-FT-HSEMs were incubated with con-DFR-DM or LMW-F-DFR-DM under air-liquid interface lifting conditions for another 28 days (Fig. S1F and Fig. 1A). Representative images and graphs illustrate the phenotype analysis of the 3D-FT-HSEMs in each group, showing the diameters and thicknesses of the constructs maintained at the indicated time points (Fig. 1). Over 28 days, con-DFR-DM incubated scaffolds showed a 94% reduction in diameter and almost complete degradation in thickness, while LMW-F-DFR-DM incubated scaffolds showed a 47% reduction in diameter and retained 25% of their thickness (Fig. 1B and C). These results suggest that LMW-F-DFR-DM might improve the maintenance of 3D-FT-HSEMs under long-term culture conditions.

LMW-F-DFR-DM positively impacts establishment of 3D-FT-HSEMs that closely resemble dermal and epidermal layers of skin

To further confirm the effects of LMW-F-DFR-DM on the histological and functional characterization of 3D-FT-HSEMs during long-term cultivation, histological analysis and functional health assessments were performed on con-DFR-DM-incubated and LMW-F-DFR-DM-incubated 3D-FT-HSEMs using IHC staining with biomarkers (Ki 67 for proliferation, K14 for early stages of keratinocyte differentiation, K10 and involucrin for terminal keratinocyte differentiation), H&E staining, and MT staining (Fig. 2). Quantitative analysis of H&E staining revealed that LMW-F-DFR-DM induced a threefold increase in epidermal thickness at day 7 compared to the 3D-FT-HSEM control group, while maintaining structural integrity until day 28 (Fig. 2A and B). Moreover, LMW-F-DFR-DM significantly attenuated dermal thickness reduction by 20% at day 14, suggesting its potential for promoting epidermal regeneration and preserving the dermal layer (Fig. 2A and C). Consistent with these findings, MT staining revealed less deterioration of the collagen scaffolds within the dermal layers of the 3D-FT-HSEMs in the presence of LMW-F-DFR-DM from 14 days to 21 days, while the collagen in the con-DFR-DM-incubated 3D-FT-HSEMs displayed more degradation after 14 days (Fig. 2A). IHC staining further confirmed that K10 and involucrin proteins were more slowly expressed in the LMW-F-DFR-DM-incubated 3D-FT-HSEMs than in the control group at 21 days (Fig. 2A). LMW-F-DFR-DM consistently enhanced Ki-67 protein expression compared to the con-DFR-DM at all assessed time points (Fig. 2A and D). Quantitative analysis of IHC staining revealed distinct proliferation patterns: $Ki\text{-}67^+$ cells in the control group increased by 26% at day 14 (relative to day 7) before declining by > 70% at day 21, whereas the LMW-F group maintained an approximately 20% increase until day 21, with cell counts decreasing by nearly 48% at day 28 (Fig. 2D). These results suggest that the application of LMW-F-DFR-DM to 3D-FT-HSEMs resulted in enhanced epidermal growth, improved dermal layer preservation, reduced collagen degradation, regulated keratinocyte differentiation, and sustained cell proliferation.

LMW-F-DFR-DM exhibits a beneficial effect on 3D-FT-HSEMs by regulating biomarkers related to epidermal/dermal quality and apoptosis

If LMW-F-DFR-DM-incubated 3D-FT-HSEMs maintain an architecture with a stable dermis and differentiated epidermis under long-term cultivation, such models would be expected to express biomarkers related to skin quality at the protein level consistent with histological results. To confirm this, western blot analyses were utilized to assess the overall quality and health of each group in the present study by examining key biomarker proteins associated with differentiation (K14, involucrin, and K10), function (LC3, p53, α-sma, fibronectin, collagen, and

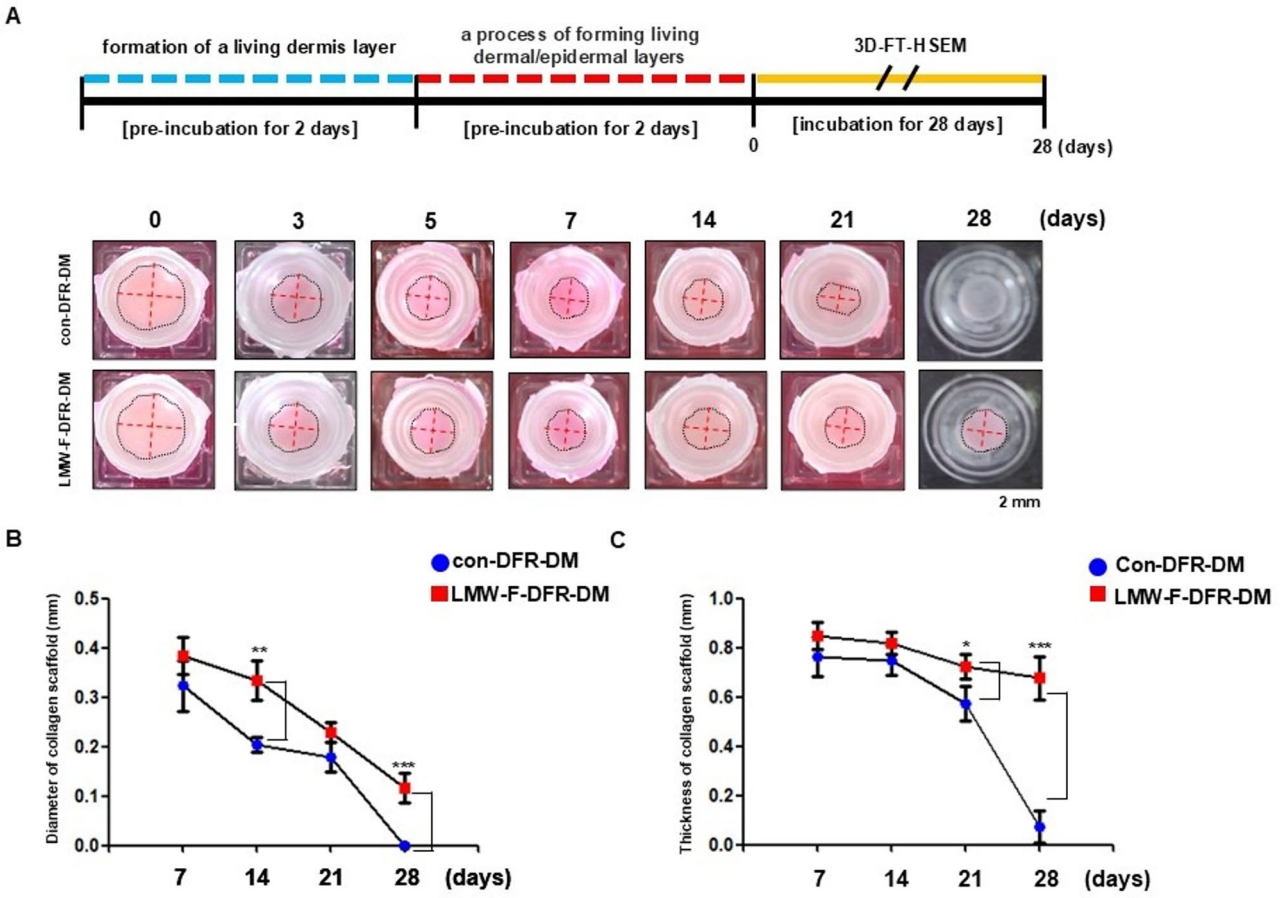

Fig. 1. Time-dependent alterations in the shape and form of 3D-FT-HSEMs under long-term culture conditions using con-DFR-DM or LMW-F-DFR-DM. (**A**) Representative images depict the morphological changes of 3D-FT-HSEMs under con-DFR-DM or LMW-F-DFR-DM from 0 to 28 days. The diameter of the representative 3D-FT-HSEM is indicated with red dashed lines. Scale bars, 2 mm. (**B**) The graph presents the diameter and shape of the 3D-FT-HSEMs (con-DFR-DM, blue; LMW-F-DFR-DM, red) at the specified time points. (**C**) The graph illustrates the thickness of the 3D-FT-HSEMs (con-DFR-DM, blue; LMW-F-DFR-DM, red) at the indicated time points. Diameter and thickness were measured using a ruler. All data were derived from three independent experiments. The data are represented as the mean ± SEM of triplicate assays expressed as a ratio of the con-DFR-DM. Statistical analysis was performed using Student's *t*-test. ** $P < 0.01$, *** $P < 0.001$ vs. corresponding controls.

Ki67), and apoptosis (pro-caspase 3, cleaved caspase 3, and PARP) (Fig. 3). The expression of K14 in the LMW-F-DFR-DM-incubated 3D-FT-HSEMs remained more stable through day 21 compared to the con-DFR-DM-incubated 3D-FT-HSEMs, while involucrin in LMW-F-DFR-DM-incubated 3D-FT-HSEMs exhibited generally lower overall expression compared to the control group (Fig. 3A and C). Similarly, LC3 expression levels were observed to be lower in the LMW-F-DFR-DM-3D-FT-HSEMs between days 14 and 21 (Fig. 3A and B). In the LMW-F-DFR-DM-incubated 3D-FT-HSEMs, there was a significant increase in α-sma expression from day 21 to day 28, while the con-DFR-DM-incubated 3D-FT-HSEMs exhibited minimal α-sma expression at all time points (Fig. 3A and B, and D). Fibronectin expression was higher in the LMW-F-DFR-DM-incubated 3D-FT-HSEMs compared to the control group. Expression of p53 sustained generally higher levels in con-DFR-DM-incubated 3D-FT-HSEMs under long-term culture, while it dramatically dropped by day 7 in the LMW-F-DFR-DM-incubated 3D-FT-HSEMs (Fig. 3A and B, and D). Ki67 and collagen in the LMW-F-DFR-DM-incubated 3D-FT-HSEM displayed more stable expression under long-term culture than the control group (Fig. 3A and B, and D). PARP and cleaved caspase-3 increased while pro-caspase 3 expression decreased in the control group. In the case of the LMW-F-DFR-DM-incubated 3D-FT-HSEMs, pro-caspase 3 expression exhibit more stability until eventually decreasing by day 28 while cleaved caspase 3 and PARP maintained minimal expression (Fig. 3A and B, and E). These findings indicate that LMW-F-DFR-DM could support the long-term cultivation of 3D-FT-HSEMs through its beneficial effects on differentiation, function, and apoptotic-related biomarkers.

LMW-F-DFR media suppresses cell proliferation, apoptosis, and aging in CCD-986sk cells

Fibroblasts are the main cells that compose the dermal layer of the skin and are responsible for producing collagen, elastin, and other proteins that provide the skin with its structure and elasticity[15]. If LMW-F-DFR-DM

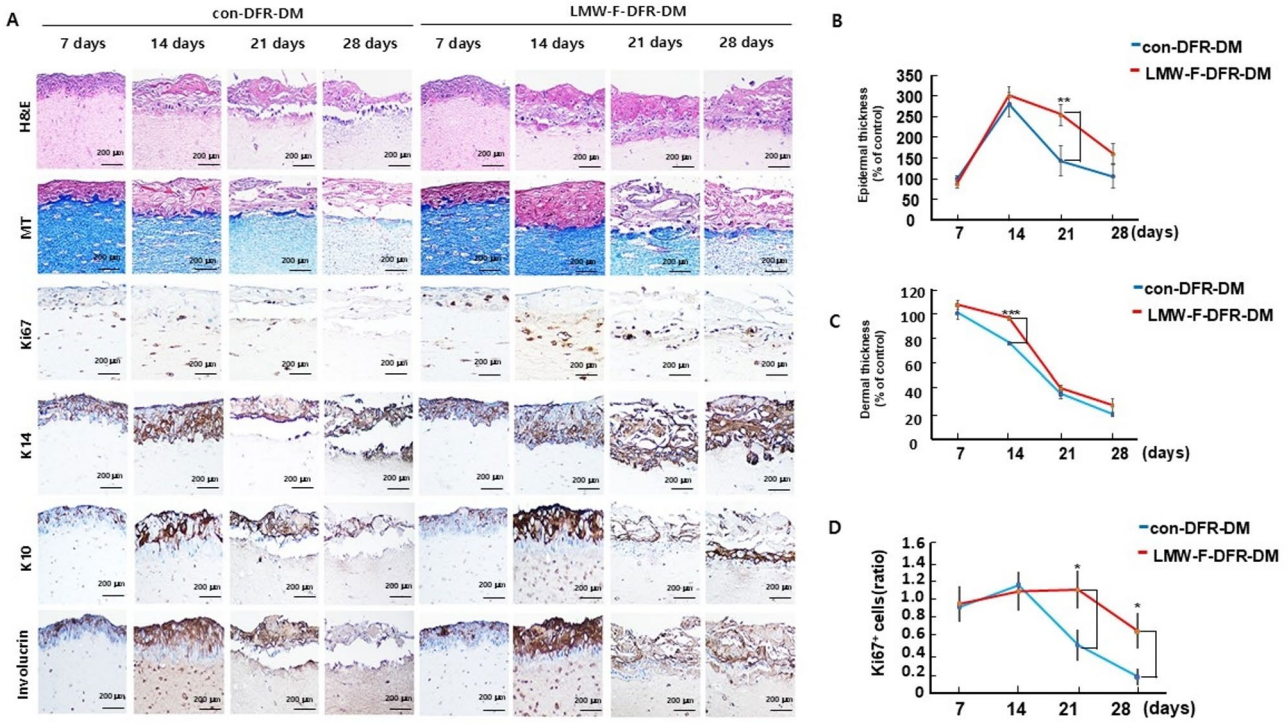

Fig. 2. The positive effects of LMW-F-DFR-DM on the structure of 3D-FT-HSEMs in cell culture over longer periods. (**A**) H&E staining, MT staining, and IHC analysis using targeted antibodies were performed for structural analysis of 3D-FT-HSEM sections in the con-DFR-DM and LW-F-DFR-DM groups at the indicated time points. Representative H&E and MT images portray the structures of the 3D-FT-HSEM sections. IHC staining with antibodies targeting Ki67, K10, K14, and involucrin show the condition of 3D-FT-HSEMs. Scale bars, 200 μm. (**B**, **C**) Graphs to indicate the thickness of the epidermal and dermal layers at the indicated times in (con-DFR-DM, blue; LMW-F-DFR-DM, red). (**C**) Graphs depicting the ratio of $Ki67^{+}$ cells compared to the con-DFR-DM. The data are represented as the mean ± SEM of triplicate assays expressed as a ratio of the con-DFR-DM. Statistical analysis was performed using Student's *t*-test. ** $P < 0.01$, *** $P < 0.001$ vs. corresponding controls.

positively impacts the overall quality and health of the dermal layer in 3D-FT-HSEMs at the protein and gene levels under long-term culture conditions, the media could be doing so through modulating dermal fibroblast function in ways that impact cell proliferation, apoptosis, and aging. To evaluate the effects of LMW-F-DFR-GM on cell proliferation and apoptosis, CCD-986sk cells were incubated with LMW-F-DFR-GM for 7 days. To test the effects of LMW-F-DFR-DM on the aging of fibroblasts, CCD-986sk cells were incubated with LMW-F-DFR-DM for 14 days. Cell proliferation and apoptosis were assessed through live and dead assays, cell counting, and live PI staining with FACS analysis. Aging was measured using a β-galactosidase assay. The results of the live and dead assays and cell counting revealed that LMW-F-DFR-GM significantly inhibited cell proliferation (approximately 1.5-fold) (Fig. 4A and C). Live PI staining with FACS analysis revealed that the LMW-F-DFR-GM-incubated fibroblasts had a reduced rate of cell death compared to the control group (Fig. 4D). Furthermore, the β-galactosidase analysis revealed that LMW-F-DFR-DM cultivation led to an approximately fivefold reduction in β-gal-positive cells, compared to the control group (Fig. 4E and F). These findings suggest that LMW-F-DFR media may have the potential to enhance the overall dermal health of 3D-FT-HSEMs by decelerating cell proliferation, cell death, and aging in fibroblasts.

LMW-F-DFR media controls cell proliferation, aging, and differentiation in keratinocytes

The interaction between keratinocyte differentiation, lysosomes, and metabolism plays a critical role in maintaining the skin barrier function and overall skin health. To evaluate the effects of LMW-F-DFR-GM on keratinocyte proliferation, HaCaT cells were incubated with LMW-F-DFR-GM for 7 days. To test the effects of LMW-F-DFR-DM on aging and differentiation, HaCaT cells were incubated with LMW-F-DFR-DM for 14 days. Keratinocyte proliferation was assessed using live and dead assays, aging was determined through a β-galactosidase assay, and differentiation was analyzed by examining lysosomal content, including biomarkers such as K14, K10, and LC3. In line with its impact on fibroblasts, LMW-F-DFR-GM suppressed the proliferation of HaCaT cells (Fig. 5A). The HaCaT cells incubated with LMW-F-DFR-DM exhibited an approximately fourfold reduction in β-gal-positive cells compared to con-DFR-DM (Fig. 5B and C). Furthermore, the upregulation of K14 and K10 proteins under differentiation conditions was inhibited by LMW-F-DFR-DM (Fig. 5D and E). Our previous study developed a simple-rapid assay using lysosomal-targeting CDy6 for long-term real-time

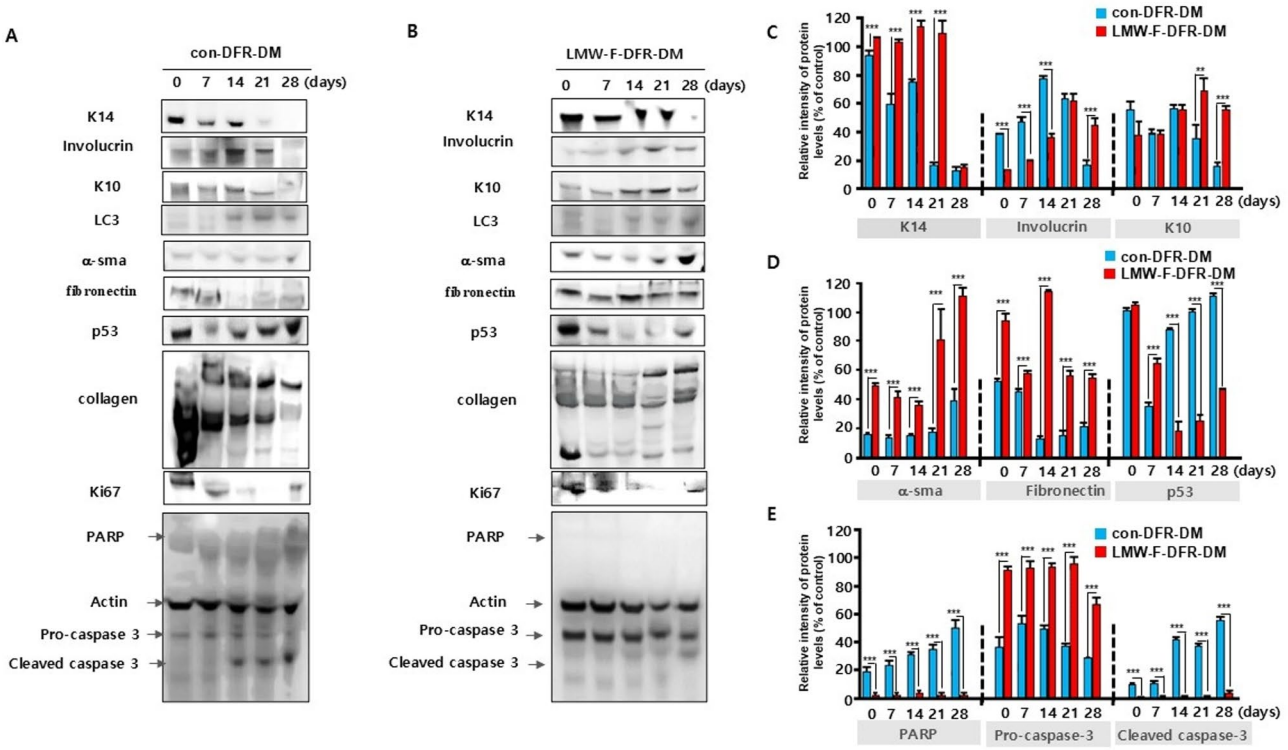

Fig. 3. LMW-F-DFR-DM delays the expression of biomarkers associated with cell death, proliferation, and keratinocyte/fibroblast function. (**A**, **B**) Western blot analysis was performed using targeted antibodies to detect molecular signatures of biomarkers associated with function of epidermal/dermal structure (K14, K10, involucrin, LC3, p53, collagen, fibronectin, α-sma), cell proliferation (Ki67), and cell death (PARP, pro-caspase 3, cleaved caspase 3) in each group of 3D-FT-HSEM at each time point. Actin was used as a loading control. (**C**–**E**) The bar graphs indicate the expression levels of targeted biomarkers derived from quantitative analysis of the western blot images. β-actin was used as an internal control to normalize protein expression. Data are expressed as the mean ± SEM of triplicate assays, relative to control. Statistical analysis was performed using Student's *t*-test. $^{**}P < 0.01$ and $^{***}P < 0.001$ versus corresponding controls.

viability assessments in 2D and 3D in vitro culture models[16]. Utilizing this assay in the present study revealed an approximately 20% lower level of CLVs and thus fewer differentiated HaCaT cells incubated in LMW-F-DFR-DM compared to the control group (Fig. 5F). These findings indicate that LMW-F-DFR media can contribute to delaying various aspects of keratinocyte function, including proliferation, aging, and differentiation.

Single-cell transcriptome profiling of 3D-FT-HSEMs incubated with LMW-F-DFR-DM identify gene expression changes associated with improved model quality and health

To further elucidate gene expression patterns and other molecular changes potentially associated with the overall quality and health of 3D-FT-HSEMs at the cellular level, a bioinformatic analysis of NGS sequences was conducted in HaCaT and CCD-986sk cells in the presence or absence of LMW-F-DFR-DM. Venn diagrams illustrate the shared up/down-regulated differentially expressed genes (DEGs) between different groups of HaCaT and CCD-986sk cells in the presence or absence of LMW-F-DFR-DM (Fig. 6A, Fig. S2). A total of 562 DEGs were identified among the average of 20,541 genes detected in each group, with 38 genes showing high expression and 251 being down-regulated in CCD-986sk cells, while 129 genes exhibited high expression and 143 were down-regulated in HaCaT cells (Fig. 6A and table. S2). To further examine the functions of DEGs in HaCaT and CCD-986sk cells both cultivated in LMW-F-DFR-DM, GO enrichment analysis was employed. Of the various GO terms generated during analysis of the DEGS, 10 terms related to the overall quality and health of artificial skin, encompassing AP (apoptotic process), CC (cell cycle), CD (collagen binding), CM (cell migration), EM (extracellular matrix), IR (inflammatory response), AG (angiogenesis), AU (autophagy), ED (epidermis development), and Ly (lysosomal metabolism) (Fig. 6B and C, Fig. S2). The analysis found up-regulated DEGs across 8 GO terms and down-regulated DEGs across all 10 GO terms (Fig. 6B and C). Moreover, a volcano plot comparing the DEGs of the HaCaT and CCD-986sk groups cultured with LMW-F-DFR-DM to those cultured with con-DFR-DM displays notable alterations in gene expression (Fig. 6D, Fig. S2). Among them, three selected genes—clusterin, decorin, and LRP1—were further analyzed using real-time qPCR, confirming their differential expression patterns in both the HaCaT and CCD-986sk cells cultured with LMW-F-DFR-DM. Consistent with the DEG results, these three genes were down-regulated compared to con-DFR-DM (Fig. 6E and F). These

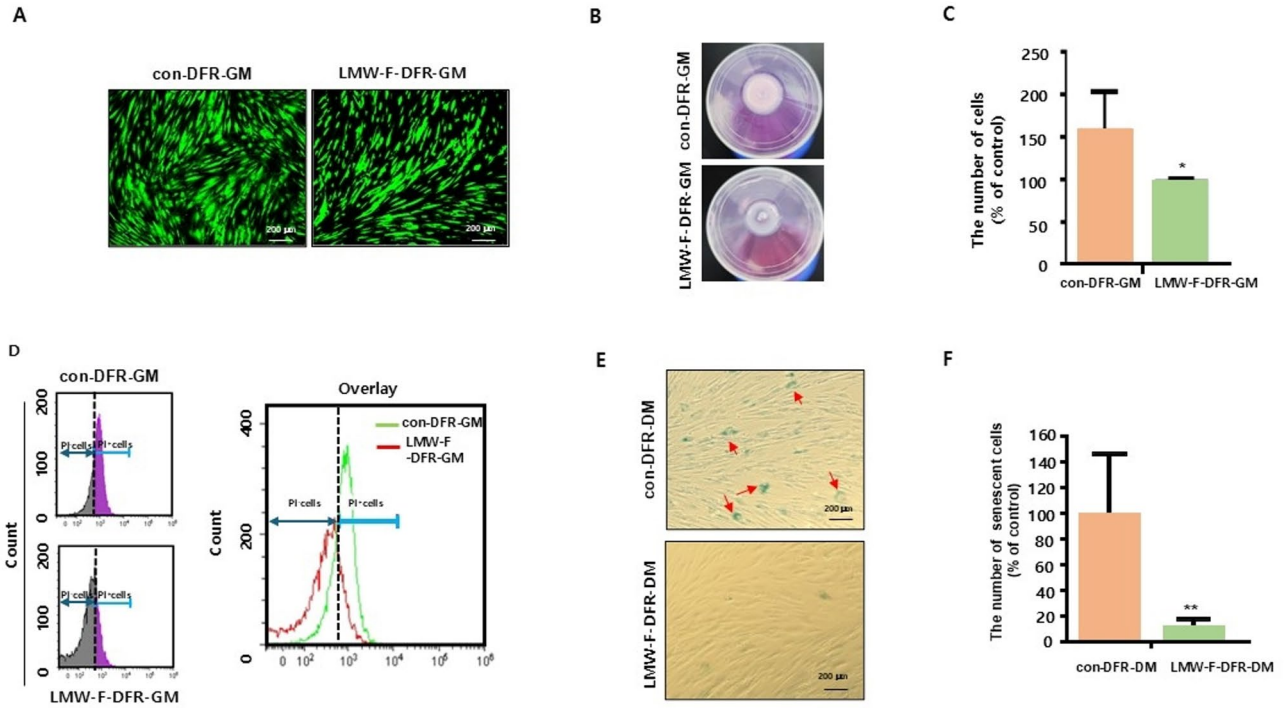

Fig. 4. LMW-DFR-GM and - DM prevent proliferation and aging of fibroblasts. (**A**) Confocal live images of live and dead assays show the CCD-986sk cells cultivated in con-DFR-GM and LMW-F-DFR-GM, with live cells indicated in green. Scale bars represent 200 μm. (**B**) CCD-986sk cells were incubated with LMW-F-DFR-GM for 7 days. Representative images show the harvested cell pellets of each group after 7 days. (**C**) The bar graph represents cell viability of CCD-986sk cells cultivated in con-DFR-GM and LMW-F-DFR-GM using a hemocytometer. (**D**) The histogram data of each group was determined by live PI staining and CytoFLEX FACS analysis. The cell population (purple area, blue line) indicates the positive PI staining to assess cell death. The overlaying histogram displays the cell viability of CCD-986sk cells cultivated in con-DFR-GM (green) and LMW-F-DFR-GM (red) at 7 days. (**E**) CCD-986sk cells were incubated with LMW-F-DFR-DM for 14 days. Brightfield images of cellular senescence-associated β-galactosidase staining of each group. The red arrows indicate the senescent cells positive for SA-β-gal staining. Scale bars, 200 μm. (**F**) The bar graph shows the number of SA-β-gal positive cells in CCD-986sk cells cultivated in con-DFR-GM (green) and LMW-F-DFR-GM (red) at 14 days. The data are represented as the mean ± SEM of triplicate assays expressed as a ratio of the con-DFR-DM. Statistical analysis was performed using Student's *t*-test. Data was analyzed using Student's *t*-test. $^{**}P < 0.01$ or $^{*}P < 0.05$ versus controls.

findings suggest that LMW-F-DFR-DM cultivation may play a role in positively impacting the overall quality and health of the dermal and epidermal layers in 3D-FT-HSEMs.

Discussion

The present study developed a novel and cost-effective method for manufacturing a 3D-FT-HSEM using commercially available HaCaT and CCD-986sk cells and designed a low-cost culture medium that can maintain the stability of 3D-FT-HSEMs for long-term in vitro culture. LMW-F-DFR-GM and -DM demonstrated superior performance in maintaining the 3D-FT-HSEMs over 28 days. Fucoidans, which are sulfated polysaccharides from brown algae such as *Fucus vesiculosus* and *Ascophyllum nodosum*, exhibit antioxidant, anti-inflammatory, anti-tumoral, anti-viral, and anti-diabetic properties[16–18]. LMW-F, a Fucoidan derivative with enhanced solubility and bioavailability, has garnered attention given its advantages over regular fucoidan[19,20]. A recent paper reported that very-low-molecular-weight fucoidan formulas (vLMW-F) with anti-proliferative and pro-apoptotic properties reduce PD-L1 surface expression in EBV Latency III and DLBCL tumoral B-cells without being toxic to normal B- and T-cells by disrupting the actin network[19]. Furthermore, our previous study illustrated that LMW-F inhibits melanoma proliferation through Bcl-2 phosphorylation and the PTEN/AKT pathway[20]. Unexpectedly, we observed beneficial effects of LMW-F, including the inhibition of fibroblast proliferation and collapse in 3D-printed collagen scaffolds. Consistent with previous findings, the addition of LMW-F to the DFR-DM resulted in slower structural collapse in the 3D-FT-HSEM compared to the control DFR-DM[20]. Histological and functional assessments confirmed that LMW-F-DFR-DM maintained the stability of the structure, collagen density, and expression of skin quality related biomarkers in 3D-FT-HSEMs. LMW-F-DFR-DM also delayed the expression of biomarkers related to epidermal/dermal quality degradation and apoptosis, thereby promoting differentiation and function as well as reducing cell death. Furthermore, LMW-F was found to suppress cell proliferation, apoptosis, and aging in fibroblasts within the dermal layer, indicating its potential benefits for

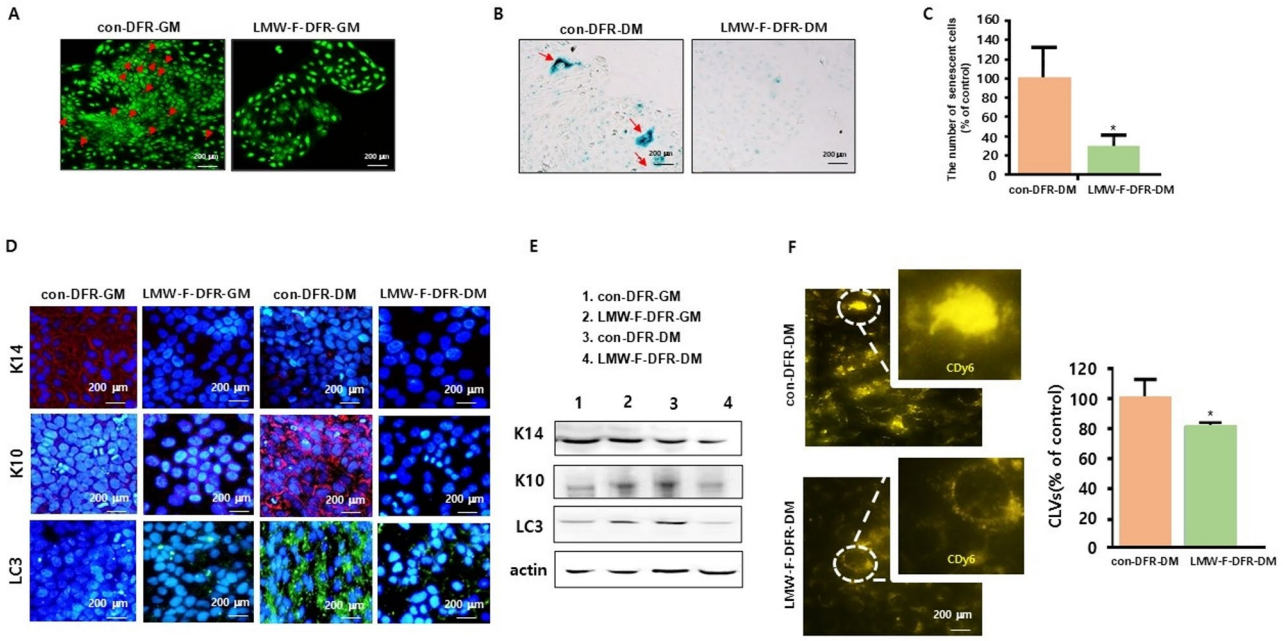

Fig. 5. LMW-DFR-GM and - DM postpone proliferation, aging, and differentiation of keratinocytes. (**A**) HaCaT cells were incubated with LMW-F-DFR-GM for 7 days. Confocal live images of live and dead assays show the con-DFR-GM-HaCaT cells and LMW-F-DFR-GM-HaCaT cells, with live cells indicated in green and dead cells indicated with red arrows. Scale bars represent 200 μm. (**B**) Cellular senescence-associated β-galactosidase staining in each group at 14 days. The red arrows indicate the senescent cells positive for SA-β-gal staining. Scale bars, 200 μm. (**C**) The bar graph shows the number of SA-β-gal positive cells. (**D**) IFS analysis for maintaining the function of HaCaT cells in each group (con-DFR-GM, LMW-F-DFR-GM, con-DFR-DM, LMW-F-DFR-DM). Scale bars represent 200 μm. (**E**) Western blot analysis for detecting molecular signatures of biomarkers in each group. (**F**) CLV assay for characterizing cell health in each group. The graph indicates the measurement of CLVs. The data are represented as the mean ± SEM of triplicate assays expressed as a ratio of the con-DFR-DM. Statistical analysis was performed using Student's *t*-test. $^{*}P < 0.05$ versus controls.

3D-FT-HSEMs. The present findings underscore the potential of a low-cost culture medium (DFR) containing LMW-F. By enhancing the stability and quality of commercially available 3D-FT-HSEMs, this medium may offer the promise of extending the shelf-life of in vitro 3D-HSMs while also facilitating the development of long-term culture models for investigating skin conditions such as skin aging and chronic disorders.

Despite the widespread use of over 115 million animals annually in laboratory research, animal experimentation remains a contentious issue with numerous ethical considerations and constraints[21]. Notable differences exist between animal and human skin in dermatological research, including variations in thickness, structure, and cell composition, which can significantly impact the absorption, distribution, metabolism, and excretion of drugs when tested on animals compared to humans[2,21]. Consequently, many promising drug candidates identified in animal studies have faced challenges progressing through clinical trials due to these disparities[2,21]. To address these challenges, in vitro 3D-HSMs are increasingly being utilized as an alternative to animal testing. In the present study, we observed that LMW-F-DFR media decreased lysosomal content, LC3 (turnover of the autophagosomal marker), and LRP1(low-density lipoprotein receptor-related protein 1) in differentiated HaCaT cells. While the specific relationship between lysosomal content in the epidermis and the biological role of cellular senescence in human skin aging is a complex subject, several studies have identified significant lysosomal changes in aging cells, such as increases in lysosomal size and number, pH neutralization, and lysosomal membrane permeabilization[22–25]. Maintaining epidermal homeostasis relies on a tightly organized process of keratinocyte proliferation and differentiation involving the remodeling of lysosomes[23–27]. For example, in the present study LRP1 gene expression was down-regulated when HaCaT cells were incubated with LMW-F-DFR-DM. This observation corroborates previous research that found LRP1 to be involved in AMP-IBP5-mediated migration and proliferation of human keratinocytes and fibroblasts[26]. Our findings are also consistent with another study reporting that an LRP-1 blockade reduced lysosome density and the level of LAMP-1 and P-glycoprotein in MCF-7, a human breast carcinoma cell line derived from pleural effusion metastasis[26]. However, the main limitation of the present study is its focus on in vitro culture conditions, which may not fully capture the dynamic interactions and responses of skin cells in a complex in vivo microenvironment. Further research utilizing animal models or clinical studies is warranted to validate the efficacy and safety of the developed 3D-FT-HSEM and our media composition. In conclusion, we described a simple and cost-effective production of 3D-FT-HSEMs and LMW-F-DFR culture media that can be used in biomedical research and in

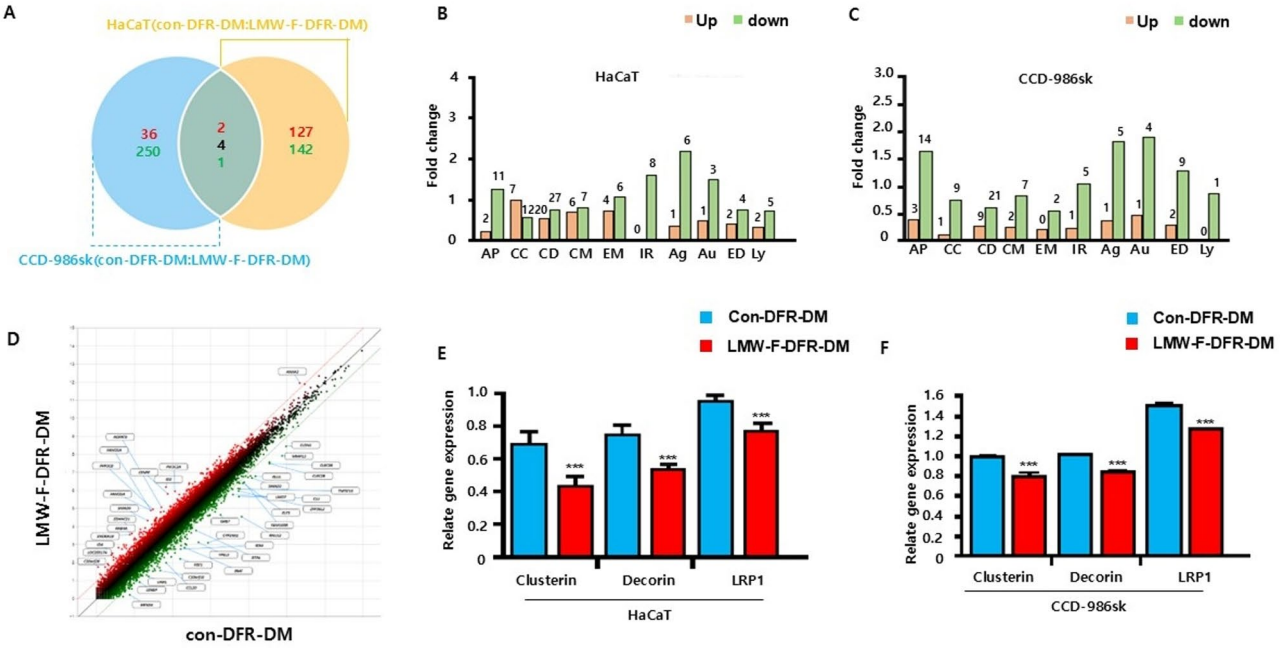

Fig. 6. Characterization of transcriptome sequencing data between control and LMW-DFR-DM in keratinocytes and fibroblasts. (**A**) Venn diagram showing the number of genes shared and unique to each group (HaCaT, yellow; CCD-986sk, blue). (**B**, **C**) GO enrichment analysis of DEGs. GO enrichment terms in 562 DEGs clustered into 10 groups (upregulated in red, downregulated in green): apoptotic process (AP), Cell cycle (CC), Cell differentiation (CD), Cell migration (CM), Extracellular matrix (EM), inflammatory response (IR), aging (Ag.), autophagy (Au.), epidermis development (ED), and lysosome (Ly). (**D**) Scatter diagram of the DEGs. (**E**, **F**) Bar graphs of qRT-PCR indicating the ratio of related targeted gene expression in HaCaT and CCD-986sk cells (con-DFR-DM, blue; LMW-F-DFR-DM, red). Data are expressed as the mean ± SEM of triplicate assays, relative to con-DFR-DM. Statistical analysis was performed using Student's *t*-test. $^{**}P < 0.01$ and $^{***}P < 0.001$ versus corresponding controls.

the healthcare industry. With global trends favoring the discontinuation of using animals in research and testing, our method could be a valuable alternative testing tool and research model for skin tissue engineering.

Materials and methods

Fabrication of 3D-FT-HSEMs and long-term cultivation

More detailed information on cell line and reagents is provided in the supplemental information section. We have modified the protocol from our previous study to manufacture the 3D-FT-HSEMs[15,19,27]. Briefly, a 3% collagen solution was mixed with CCD-986sk cells (2.5×10^5/ml) to generate a uniform and stable 3D dermal layer-on-frame construction with polyether sulfone (PES) membrane filters (circle type, pore size 0.45 µm) using the extrusion printing method with a 3DX Printer (T&R Biofab Co. Ltd, Siheung, Korea) (Fig. S1). Following gelation, the 3D dermal layer-on-frame structures with PES membrane filters were cultured in con-DFR-GM and LMW-F-DFR-GM at 37 °C in a 5% CO_2 incubator for pre-incubation 2 days. Subsequently, HaCaT cells (2×10^5/per insert) were seeded onto these 3D dermal layer-on-frame structures. The constructions were submerged for 2 days in con-DFR-GM and LMW-F-DFR-GM. After this pre-incubation, the inserts containing the constructs were transitioned to an air-liquid interface culture in con-DFR-DM and LMW-F-DFR-DM for 28 days (Fig. 1A and Fig. S1). The culture medium was refreshed every seven days, and samples were collected at specified time points. After the fabrication of the 3D-FT-HSEMs, the diameter and thickness of collagen scaffolds were measured at 0, 3, 5, 7, 14, 21, and 28 days with a ruler after the fabrication of the 3D-FT-HSEMs.

Hematoxylin and Eosin (H&E), masson's trichrome staining (MT), immunohistochemistry (IHC) staining, and Immunofluorescence staining (IFS)

To assess the architecture of the 3D-FT-HSEMs under long-term cultivation, we conducted H&E, MT, and IHC staining[15,19,27]. The H&E staining protocol involves deparaffinization and rehydration of formalin-fixed paraffin-embedded tissue sections, followed by staining with Harris hematoxylin for nuclear staining and eosin Y for cytoplasmic and extracellular staining. Subsequently, the slides undergo dehydration, clearing, mounting with DPX mountant, and sealing for observation and analysis under a light microscope. The MT staining protocol includes deparaffinization and rehydration of sample sections, staining with Weigert's iron hematoxylin for nuclei, Biebrich scarlet-acid fuchsin for cytoplasm and muscle fibers, and phosphomolybdic acid for collagen fibers. Aniline blue is used for counterstaining to highlight collagen fibers and the extracellular matrix. Following staining, the sections are dehydrated, cleared, and mounted for microscopic examination. IHC staining utilizes

a heated target retrieval solution and slides are incubated with peroxidase-blocking solution for 15 min at room temperature (RT). Primary antibodies (1:100 dilution) are incubated overnight at 4 °C in a humid chamber. The horseradish peroxidase (HRP)-conjugated secondary antibody was detected using the Real Envision system kit (Dako, Carpinteria, CA, USA) for 30 min at RT. The immunoreaction was developed for one minute, followed by hematoxylin counterstaining. Brightfield photographs were captured using a Leica light microscope DMI 5000B (Leoca, Wetzlar, Germany). IFS-labelled coverglasses with HaCaT cells were incubated with primary antibodies (1:100). After nuclear DAPI staining, immunostained cells were imaged using Olympus FV1200 confocal microscope with 405, 473, 559, and 635 nm laser lines.

Cell survival and proliferation assay

Cell viability and proliferation assays were prepared and conducted using live and dead staining, cell counting, live PI staining, and CLV assay, as previously described[15,19,27]. Absorbance for each dye was measured using a spectrometer (Emax; Molecular Devices, Sunnyvale, CA, USA). FACS analysis was carried out using a CytoFLEX flow cytometer (Beckman Coulter Life Sciences).

Senescence-activated β-galactosidase staining

HaCaT and CCD-986sk cells (1×10^4) were plated in 35 mm diameter plates and treated with LMW-F-DFR-DM for 14 days. Senescence-activated expression of β-galactosidase activity was detected using the cellular senescence β-Gal assay kit (Cell Signaling Technology, Danvers, MA, USA) following the manufacturer's protocol and observed under a microscope.

Statistical analysis

Student's *t*-tests (for comparisons of two groups) was used for the statistical analyses. SPSS software ver. 17.0 (SPSS, Chicago, IL) was used. A value of $P < 0.05$ was considered significant. Data are expressed as means ± standard error of the mean (SEM). Data analysis was carried out using GraphPad Prism software (GraphPad Software Inc). $^*P < 0.05$–0.01, $^{**}P < 0.01$–0.001, and $^{***}P < 0.001$ vs. corresponding controls. All error bars represent a standard deviation of three or more biological replicates.

Data availability

All data generated or analyzed during this study are included in this published article [and its supplementary information files]. The datasets used and/or analyzed during the current study available from the corresponding author (phdjeongym12@tukorea.ac.kr) on reasonable request.

Received: 1 February 2025; Accepted: 2 June 2025
Published online: 02 July 2025

References

1. Domínguez-Oliva, A. et al. The importance of animal models in biomedical research: current insights and applications. *Anim. (Basel).* **13**, 1223 (2023).
2. Poh, W. T. & Stanslas, J. The new paradigm in animal testing - 3Rs alternatives. *Regul. Toxicol Pharmacol.* **153**, 105705 (2024).
3. Wistner, S. C., Rashad, L. & Slaughter, G. Advances in tissue engineering and biofabrication for *in vitro* skin modeling. *Bioprinting* **35**, e00306 (2023).
4. Jorgensen, A. M. et al. Multicellular bioprinted skin facilitates human-like skin architecture in vivo. *Sci. Transl Med.* **15**, eadf7547 (2023).
5. Słoczyńska, K. et al. Evaluation of two novel hydantoin derivatives using reconstructed human skin model episkin™: perspectives for application as potential sunscreen agents. *Molecules* **27**, 1850 (2022).
6. Morales, M., Pérez, D., Correa, L. & Restrepo, L. Evaluation of fibrin-based dermal-epidermal organotypic cultures for in vitro skin corrosion and irritation testing of chemicals according to OECD TG 431 and 439. *Toxicol. Vitro*, 89–96 (2016).
7. Suhail, S. et al. Engineered skin tissue equivalents for product evaluation and therapeutic applications. *Biotechnol. J.* **14**, e1900022 (2019).
8. Shi, X. L. et al. Optimization of an effective directed differentiation medium for differentiating mouse bone marrow mesenchymal stem cells into hepatocytes in vitro. *Cell. Biol. Int.* **32**, 959–965 (2008).
9. Petry, L. et al. Directing adipose-derived stem cells into keratinocyte-like cells: impact of medium composition and culture condition. *J. Eur. Acad. Dermatol. Venereol.* **32**, 2010–2019 (2018).
10. Font, J. et al. A new three-dimensional culture of human keratinocytes: optimization of differentiation. *Cell. Biol. Toxicol.* **10**, 353–359 (1994).
11. Sakamoto, H., Nishikawa, M. & Yamada, S. Development of tight junction-strengthening compounds using a high-throughput screening system to evaluate cell surface-localized claudin-1 in keratinocytes. *Sci. Rep.* **14**, 3312 (2024).
12. Savoji, H., Godau, B., Hassani, M. S. & Akbari, M. Skin tissue substitutes and biomaterial risk assessment and testing. *Front. Bioeng. Biotechnol.* **6**, 86 (2018).
13. Schmidt, F. F., Nowakowski, S. & Kluger, P. J. Improvement of a Three-Layered *in vitro* skin model for topical application of irritating substances. *Front. Bioeng. Biotechnol.* **8**, 388 (2020).
14. Boraldi, F. et al. The role of fibroblasts in skin homeostasis and repair. *Biomedicines* **12**, 1586 (2024).
15. Kang, C., Yun, W. S. & Jeong, Y. M. A simple and rapid assay of lysosomal-targeting CDy6 for long-term real-time viability assessments in 2D and 3D in vitro culture models. *Sci. Rep.* **13**, 23038 (2023).
16. Wang, L. et al. Antioxidant and anti-photoaging effects of a fucoidan isolated from Turbinaria ornata. *Int. J. Biol. Macromol.* **225**, 1021–1027 (2023).
17. Achmad, A. A. et al. Development of dissolving microneedles loaded with fucoidan for enhanced anti-aging activity: an in vivo study in mice animal model. *Eur. J. Pharm. Biopharm.* **114362** (2024).
18. Saliba, J. et al. Anti-proliferative and pro-apoptotic vLMW fucoidan formulas decrease PD-L1 surface expression in EBV latency iii and DLBCL tumoral B-cells by decreasing actin network. *Mar. Drugs.* **21**, 132 (2023).
19. Park, M., Bang, C., Yun, W. S. & Jeong, Y. M. Low-molecular-weight fucoidan inhibits the proliferation of melanoma via Bcl-2 phosphorylation and PTEN/AKT pathway. *Oncol. Res.* **32**, 273–282 (2023).

20. Storz, M. A. & Dean, E. Status of animal experimentation in nutrition and dietetic research: Policies of 100 leading journals and new approach methodologies. *Account. Res.* 1–19 (2024).
21. Randall, M. J., Jüngel, A., Rimann, M. & Wuertz-Kozak, K. Advances in the biofabrication of 3D skin *in vitro*: healthy and pathological models. *Front. Bioeng. Biotechnol.* **6**, 154 (2018).
22. Tan, J. X. & Finkel, T. Lysosomes in senescence and aging. *EMBO Rep.* **24**, e57265 (2023).
23. He, Y. et al. Targeting lysosomal quality control as a therapeutic strategy against aging and diseases. *Med. Res. Rev.* **44**, 2472–2509 (2024).
24. Mahanty, S. et al. Keratinocyte differentiation promotes ER stress-dependent lysosome biogenesis. *Cell. Death Dis.* **10**, 269 (2019).
25. Chieosilapatham, P., Yue, H., Ikeda, S., Ogawa, H. & Niyonsaba, F. Involvement of the lipoprotein receptor LRP1 in AMP-IBP5-mediated migration and proliferation of human keratinocytes and fibroblasts. *J. Dermatol. Sci.* **99**, 158–167 (2020).
26. Henry, A. et al. The endocytic receptor protein LRP-1 modulate P-glycoprotein mediated drug resistance in MCF-7 cells. *PLoS One.* **18**, e0285834 (2023).
27. Jeong, Y. M. et al. 3D-printed collagen scaffolds promote maintenance of cryopreserved patients-derived melanoma explants. *Cells* **10**, 589 (2021).

Acknowledgements
We would like to thank Diacorda Amosapa for her careful English proofreading and editing.

Author contributions
J.Y.M, W.S.Y, and S.J.H contributed to the conception of the research. J.Y.M performed all experiments, analyzed all data, and wrote the article. J.Y.M and W.S.Y designed the research and edited the manuscript. J.Y.M and S.J.H. are the corresponding authors. All authors reviewed the manuscript and approved of the final manuscript.

Funding
This research was supported by the Priority Research Centers Program through the National Research Foundation of Korea (NRF) funded by the Ministry of Education, Science and Technology (Grant 2017R1A6A03015562 and RS-2023-00237386).

Declarations

Competing interests
The authors declare no competing interests.

Additional information
Supplementary Information The online version contains supplementary material available at https://doi.org/10.1038/s41598-025-05461-8.

Correspondence and requests for materials should be addressed to Y.-M.J. or J.-H.S.